Int J Adv Manuf Technol (2011) 57:575–584
DOI 10.1007/s00170-011-3305-7

ORIGINAL ARTICLE

Modeling of surface roughness effect on dry contact friction in metal forming

Daw-Kwei Leu

Received: 24 November 2010 / Accepted: 27 March 2011 / Published online: 20 April 2011

Abstract Interfacial conditions such as friction and roughness substantially affect the process characteristics of metal forming. This study developed a dry friction model that accounted for the adhesion and interference effects of surface roughness. A sliding friction coefficient was suggested to provide fundamental information about the interfacial conditions of the contact surface. The proposed model was easily verified by published experiments and predicted values agreed with experimental results. Accordingly, friction coefficient μ clearly increased as relative roughness R_m (=roughness of tool R_a^T/roughness of workpiece R_a^M, measured as interference effect) increased. Simulations confirmed that the friction coefficient μ decreased as dimensionless stress S_m (=contact pressure p_m/tensile strength σ_u^0) increased at small strain hardening exponent n-values. Under the conditions of large n and small R_m values, the friction coefficient μ initially decreased and then increased. It then slightly decreased as dimensionless stress S_m increased. However, this trend became less apparent as relative roughness R_m increased since friction coefficient μ simply decreased.

Keywords Friction · Roughness · Interference · Adhesion

1 Introduction

The most significant effect on surface contact is resistance when sliding, which is the meaning of contact friction. Contact friction is an important issue of manufacturing, especially in metal cutting and metal forming. However, the friction of metal cutting is not similar to the usual sliding case, which value is exceptionally high and varies with tool geometry, thermal effect, and other cutting conditions. The present work mainly investigates the effect of surface roughness on dry contact friction in metal forming via a conventional sliding friction law. Contact friction is due to forces that arise from the interactions of asperities in sliding contact. In the contact layer, interactions among asperities, together with adhesion, always occur and will commonly be the main cause of friction. However, the contribution of interference of asperities may or may not be significant. Its effect depends on the surface roughness and the relative hardness of the contact surfaces. Two interactions of asperities are conventionally identified adhesion and deformation. These effects associated with friction are not simply additive, but are interactive. Since all surfaces of mechanical parts are to some degree rough once manufactured, the modeling of contact between these rough surfaces becomes extremely important and leads to an enhanced understanding of contact friction between surfaces. When two rough surfaces are pressed together under a load, only the asperities on the surface are in contact. Thus, the asperities of surfaces often have very high loads, often causing surface yielding. Therefore, purely elastic contact models of rough surfaces are not always adequate under severe loading.

Notably, two different models are typically utilized to analyze contacting asperities. One model is indentation loading in which a rigid sphere penetrates a deformed plane such as the study reported by Leu [1], and the other model is the reverse case, in which a deformed sphere is loaded against a rigid flat such as the study reported by Leu [2]; these models are employed to investigate the characteristics

D.-K. Leu (✉)
Department of Mechanical Engineering, Technology and Science Institute of Northern Taiwan,
No.2, XueYuan Road, Beitou,
Taipei 112, Taiwan, Republic of China
e-mail: dkleu@tsint.edu.tw

of contact. However, this work is to develop a method of measuring the equivalence between flat interfaces and for describing their geometric properties when evaluating contact friction via a conventional friction mode.

Greenwood and Williamson [3] pioneered the study of frictionless contact between a hemisphere and a rigid flat (the Greenwood and Williamson (GW) model) applied the Hertz contact solution to model an entire contact surface of elastic asperities. To supplement the GW model, many elastic-plastic asperity models have been devised. Many plastic contact models are based on the Abbott and Firestone model [4], but neglect volume conservation of plastic deformation. Plastic contact of surfaces is a fundamental problem in the contact mechanics of severe loading. Any understanding of friction must be rooted in an understanding of contact mechanics. During contact, asperity interactions combined with adhesion always occur and are often the primary cause of friction. Chang et al. [5] applied the GW model to an elastic-plastic contact (CEB) model to estimate the static friction of two rough surfaces in contact. Elastic-plastic finite element solutions, such as the sliding inception of a spherical contact developed by Kogut and Etsion [6] and the elastic-plastic contacting rough surfaces developed by Kogut and Etsion [7], are applied to predict a better static friction coefficient than that predicted by Chang et al. [5]. Cohen et al. [8] then studied the elastic-plastic spherical contact of rough surfaces under combined normal and tangential loading with full stick contact condition.

Previously, most friction models have been based on experimental observations. However, the success of the well-known adhesion theory of Bowden and Tabor [9] has motivated several researchers to develop more advanced analyses of the plastic deformation of asperities at low normal pressures. Orowan [10] was the first to develop a friction model at high pressures. It is more complex than the model at low pressures because of the extensive interaction of deformed asperities and plastic constraints. Wanheim et al. [11], Bay and Wanheim [12], and Wanheim and Bay [13] performed a series of studies to develop a model that included relative sliding and friction stress in the asperity contact. Bay [14] further considered the asperity slope in an analytical form, using the above friction models. Greenwood and Rowe [15] had emphasized the effect of bulk plasticity on the flattening of surface asperities. Sheu and Wilson [16] and Wilson and Sheu [17] studied the effect of bulk plasticity on asperity flattening for surfaces with longitudinal roughness. Sutcliffe [18] elucidated the flattening of transverse and longitudinal asperities by performing a slip-line field analysis.

As the measurement of friction, Azushima [19] developed a flat tool-drawing apparatus using a video system to observe directly the contact behavior at the interface in sheet metal forming. Gong et al. [20] proposed a probe test method for detecting the friction conditions of the interfaces between the tools and the workpiece in the sheet drawing process. Xie and Wilfams [21] proposed a method for predicting the friction coefficient and wear rate of a soft surface that comes into contact with a rough hard surface with random asperities. Lovell and Deng [22] introduced an experimental procedure to characterize the sliding friction between a hard tool and a deformable workpiece using a pin-on-disk tribometer.

Furthermore, Cho and Ngaile [23] developed an inverse analysis approach to determine the flow stress and friction at the tool/workpiece interface simultaneously from a single series of material tests using the finite element method. Carpinteri and Paggi [24] proposed an interpretation of the size effect on the friction coefficient to explain frictional phenomena over all the scales. Stachowiak and Batchelor [25] concluded that the elastic and plastic deformation of asperities is the primary cause of friction. Solid-state adhesion is the second cause, and causes very high friction. Viscous drag, resulting from hydrodynamic lubrication, is the third and causes low frictional resistance. Lanzon et al. [26] experimentally studied the effects of lubricant, surface finish, contact pressure, sheet metal coating, and draw speed on friction. Weidel and Enget [27] reported the effect of surface topography of tool and workpiece on friction by using new functional 3D parameters of surface based on the developed software, WinSAM, during metal forming. Menezes et al. [28] performed an experiment using an inclined pin-on-plate sliding apparatus to investigate the effect of grinding mark directionality, i.e., surface texture, on friction coefficient and transfer layer formation during sliding contact. Menezes et al. [29] theoretically investigated the effect of friction coefficient on metal forming by FE method, simulating three kinds of compression tests on cylindrical Al–Mg alloy in which friction coefficient is assumed as constant in upper die–workpiece interface but various in lower die–workpiece interface. Menezes et al. [30] experimentally investigated the effect of surface texture on friction coefficient by using an inclined pin-on-plate sliding tester under dry and lubricated conditions, and observed that friction coefficient and transfer layer formation depend primarily on the surface texture of hard surface. On the materials aspect, Rigney [31] used complementary characterization techniques to reveal a wide variety of near-surface features on ductile materials subjected to sliding. All of these depend on a few basic processes: plastic deformation, transfer, interactions with the environment, and mechanical mixing. Bonny et al. [32] revealed a significant effect of microstructure of secondary WC phase on wire EDM behavior and frictional characteristics by performing a dry reciprocating sliding experiment using a

pin-on-plate testing rig. Diaz de Cerio et al. [33] reported the tribological properties of magnetron-sputtered WC-C and chemical vapor-deposited diamond-like carbon films coated onto hard metal surfaces when sliding on aluminum foil under different temperatures. This study addressed the evolution of friction coefficient in the interface of coated hard metal and aluminum foil under dry lubrication condition using a ball-on-disk test.

Recently, strong industrial demand for increased integration and packaging densities of electronic devices has resulted in the miniaturization of manufacturing processes. When reducing a conventional forming process to microscale, the so-called size effect must be considered. Microstructural features such as grain size and boundary and interfacial conditions such as friction and roughness can substantially affect process characteristics. Despite recent technological advances, theoretical or numerical solutions are still needed for process optimization. Therefore, valid modeling tools are needed to fabricate products at this scale. The major concerns when adapting forming modeling tools to this field of application are the increased importance of geometric surface features and their effects on material flows, which must be accurately estimated. Control and predictability determine the functionality, costs, and quality of produced parts. A friction model that accounts for the size effect on the sliding coefficient is needed to provide fundamental information about the interfacial conditions of the contact surface.

The idea of modeling friction from the interface geometry between workpiece and tool has attracted the attention of many researchers, but an empirical measure of the relationship between friction and the tool roughness profile is still needed. Previous works such as Edwards and Halling [34], Wanheim and Abildgaard [35], and Avitzur et al. [36] used physical modeling, slip line field, and upper bound techniques. Deformation in workpiece asperities has also been studied intensively. Osakada and Matsumoto [37] developed an approach for modeling surface friction but did not establish the empirical relationship needed to simulate forming processes. Lee et al. [38] designed a sheet metal friction tester and proposed a friction model that considered lubricant viscosity and surface roughness for use in finite element analysis of sheet metal forming processes. The relationship between friction coefficient and process parameters, lubricant viscosity and surface roughness was quantified by least squares method on the basis of experimental results. Becker et al. [39] described an alternative approach for describing friction in terms of geometric surface roughness. The relationship between surface geometry and friction was established by ring test. Mahrenholtz et al. [40] tested the effect of surface roughness on friction during metal forming processes by applying a non-local friction law. Accordingly, a measure of the effect of surface roughness on Coulomb friction was proposed. Jeon and Bramley [41] described friction and friction factors in terms of the geometric surface roughness of the tool for simulating microforming. This finite element-based model has been validated experimentally in metal forming problems in terms of load by using ring test and actual surface measurements. Menezes et al. [42] investigated the effect of roughness parameters on friction coefficient during sliding by using an inclined pin-on-plate sliding tester with lubrication. The experimental results showed that, in all tested materials, the average friction coefficient was determined by the mean slope of the surface roughness profile.

This work developed a simple dry contact model of interference and adhesion effects caused by roughness (or asperities) in microview to model sliding friction as measured by Amonton–Coulomb friction law. The model assumed that dry friction results from adhesion in the normal contact and the interference in the lateral contact by the contact interaction of roughness, which applied to actual physical properties of the surface. A roughness model was established to explore how interference affects contact friction. The sliding friction coefficient predicted by the proposed model was compared with the measured values by ring compression test under dry conditions. To characterize contact friction accurately, the effects of material property and surface roughness were examined. The model therefore actually revealed the relationships between surface roughness and contact friction.

2 Basic analysis

For forming modeling, contact analysis must be sufficiently realistic. Therefore, tools are modeled as rigid bodies, and the workpiece material was modeled as a deformable body. Based on the physical contact behavior of surfaces with varying roughness (asperities) between tools and workpiece, the proposed model depicted the adhesion effect associated with normal contact (Fig. 1) and the interference effect associated with lateral contact (Fig. 2). The model assumed that asperities of both tool and workpiece are simple cantilever beams with constant section. The average surface roughness of the tool (the rigid body) was denoted by R_a^T, which was assumed to remain constant during deformation. The average surface roughness of the workpiece (the deformable body) was denoted by R_a^M and varied during deformation.

When the free surface of a workpiece deforms, grain size and plastic strain induce a coarse surface layer, i.e., surface roughness increases. The free surface roughness caused by metal deformation was determined by the following

At a certain contact,

$\overset{M}{Ra}$: roughness of deformable material

$\overset{T}{Ra}$: roughness of rigid-like material (tool)

Fc : compressive load as a normal force in contact area

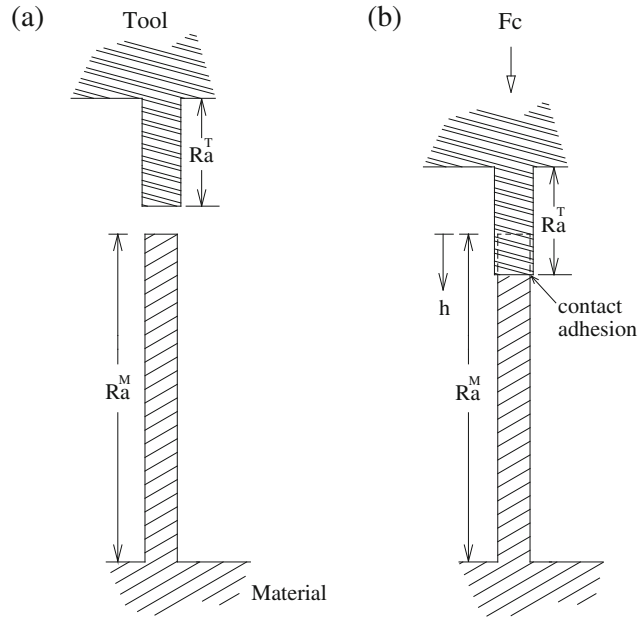

Fig. 1 **a** Before and **b** after adhesion contact

empirical relationship:

$$R_a^M = \overline{R}_a^M + \widetilde{c}\,\varepsilon_m D_g \tag{1}$$

where $\overline{R}_a^M$ was the initial material roughness, $\widetilde{c}(\approx 1)$ was a constant, ε_m was deformation strain, and D_g was the grain size of the material.

The friction law proposed by Shaw [43] was applied as

$$\mu = \alpha \frac{\tau_f}{p} \tag{2}$$

where normal stress was $p=3p_r$ according to Brinell hardness test mentioned in reference [44], p_r was real contact stress, and $\alpha(=A_r/A_a)$ was real contact area ratio, in which A_r was real contact area, and A_a was apparent area, defined as

$$\alpha = \tanh\left(2\frac{p_m}{\sigma_u}\right) \tag{3}$$

proposed by Leu [45], p_m was apparent contact stress such that $p_m Aa = p_r A_r$ or $p_m/\alpha = p_r$; therefore, $0 \le p_m \le \sigma_u = C(2n)^n$. The true tensile strength in terms of true stress was defined as $\sigma_u = C(2n)^n$ for the axial compression condition that critical axial strain $\varepsilon_u = 2n$ due to $\varepsilon_u = 2\varepsilon_\theta$ and $\varepsilon_\theta = n$ under the critical condition, ε_θ was circumference strain, and n was strain hardening exponent. The mean friction stress τ_f on the contact surface was defined as

$$\tau_f = \beta\tau_s + (1-\beta)\sigma_i \tag{4}$$

in which τ_s was the shear strength of material and equals $\tau_s = \sigma_u^0/2 = C(n/e)^n/2$ in which σ_u^0 was the tensile strength of material, β was adhesion factor as shown by the percentage of adhesion in contact area, and $\beta=\alpha$. The term σ_i was interference stress due to roughness interaction distributed on $(1-\beta)$ contact area.

Thus, the friction coefficient μ can be rewritten as

$$\mu = \frac{\alpha^2}{3}\frac{1}{\left(\frac{p_m}{\tau_s}\right)}\left[\beta + (1-\beta)\left(\frac{\sigma_i}{\tau_s}\right)\right] = \frac{\alpha^2}{6}\frac{1}{\left(\frac{p_m}{\sigma_u^0}\right)}\left[\beta + (1-\beta)\left(\frac{\sigma_i}{\tau_s}\right)\right] \tag{5}$$

where $0 \le \left(p_m/\sigma_u^0\right) \le (2e)^n$, and the interference stress σ_i due to roughness was assumedly a function of $\sigma_i = f\left(h, p_m, \tau_s, R_a^T, R_a^M\right)$, in which h was impression of normal contact.

The dimensionless interference stress σ_i/τ_s could then be deduced from the three following conditions.

Fig. 2 **a** Interference contact model; **b** at the condition of $0 \le h \le R_a^T$ and **c** at the condition of $R_a^T \le h \le (1-e^{-2n})R_a^M$

At a certain contact, $\overset{T}{Ra}$: roughness of rigid-like material, $\overset{M}{Ra}$: roughness of deformable material.

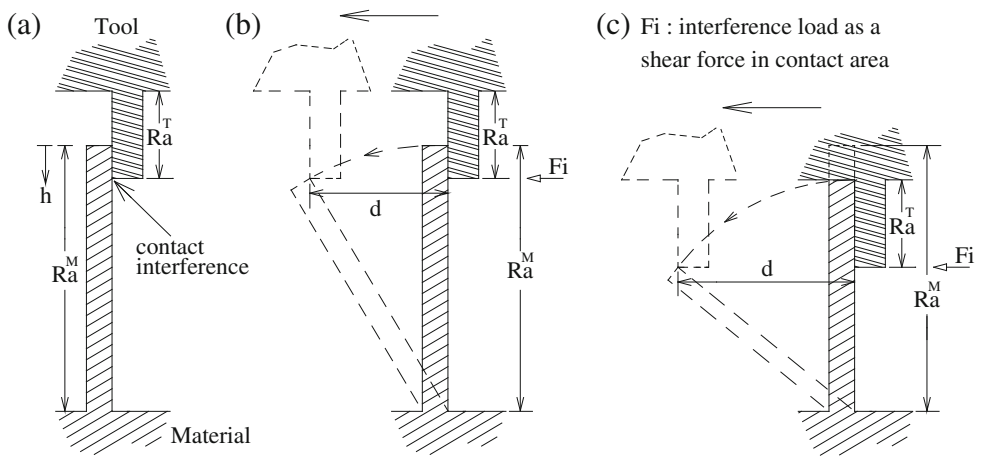

Condition 1: $0 \le h \le R_a^T$ shown in Fig. 2b

According to the elementary geometric analysis in Fig. 2b, deflection in cantilever beam d can be formulated as

$$d = R_a^M\left(1-\frac{h}{R_a^M}\right)\sqrt{2\frac{h}{R_a^M}-\left(\frac{h}{R_a^M}\right)^2} \tag{6}$$

As R_a^M (asperity height) is reduced to the critical condition of $R_a^M e^{-2n}$ under axial compression (normal contact), the critical d, d_c, can be written as

$$d_c = R_a^M\left[\frac{1}{1+e^{2n}\left(R_a^T/R_a^M\right)}\right]\sqrt{2e^{-2n}\frac{R_a^T}{R_a^M}+\left(\frac{R_a^T}{R_a^M}\right)^2} \tag{7}$$

Comparison of d with d_c reveals the following relationship:

$$\frac{d}{d_c} = \left(1-\frac{h}{R_a^M}\right)\left[1+e^{2n}\frac{R_a^T}{R_a^M}\right] \times\sqrt{\frac{2\left(h/R_a^M\right)-\left(h/R_a^M\right)^2}{2e^{-2n}\left(R_a^T/R_a^M\right)+\left(R_a^T/R_a^M\right)^2}} \tag{8}$$

Elementary analysis of rigid plastic deformation of work-hardening material for a cantilever beam with a single force shows that the relationship d/d_c can be rewritten as

$$\frac{d}{d_c} = \left[\frac{\sigma_i}{\sigma_u^0}\frac{h}{R_a^T}\left(\frac{d_m}{d_x}\right)^2\right]^{1/n} \left[\frac{d_m}{d_x}\frac{1-\left(h/R_a^M\right)}{e^{-2n}}\right]^{2+1/n} \tag{9}$$

where d_x and d_m denote asperity diameter under a certain compression and critical condition, respectively, where asperity was assumedly a round bar. Under the constant volume law of plasticity, d_m/d_x can be written as

$$\frac{d_m}{d_x} = \sqrt{\frac{1}{e^{-2n}+\left(R_a^T/R_a^M\right)}} \tag{10}$$

According to Eq. 9, σ_i/τ_s can then be written as

$$\frac{\sigma_i}{\tau_s} = 2e^{-2n(1+2n)}\left(\frac{h}{R_a^M}\right)^{-1}\left[1+e^{2n}\left(\frac{R_a^T}{R_a^M}\right)\right]^n\left(1-\frac{h}{R_a^M}\right)^{-1-n}\left[e^{-2n}+\left(\frac{R_a^T}{R_a^M}\right)\right]^{1+n/2} \left\{\left[2\left(\frac{h}{R_a^M}\right)-\left(\frac{h}{R_a^M}\right)^2\right]\Big/\left[2e^{-2n}\left(\frac{R_a^T}{R_a^M}\right)+\left(\frac{R_a^T}{R_a^M}\right)^2\right]\right\}^{n/2}\left(\frac{R_a^T}{R_a^M}\right) \tag{11}$$

which was a function of dimensionless variable h/R_a^M under the certain values of n and relative roughness R_a^T/R_a^M; and $h/R_a^M = 1-e^{-(p_m/C)^{1/n}}$ for the axial compression, in which $p_m/C = \left(p_m/\sigma_u^0\right)\left(\sigma_u^0/C\right) = \left(p_m/\sigma_u^0\right)(n/e)^n$ and $0 \le \left(p_m/\sigma_u^0\right) \le (2e)^n$. Then, σ_i/τ_s can also be represented as a function of $\left(p_m/\sigma_u^0\right)$. The surface roughness values $\left(R_a^T/R_a^M\right)$ can then be expressed in terms of the friction coefficient via Eq. 5.

Condition 2: $R_a^T \le h \le (1-e^{-2n})R_a^M$ shown in Fig. 2c

As in case 1, the deflection of cantilever beam with short length due to axial compression can be described as

$$d = R_a^M\left[\frac{1}{1+e^{(p_m/C)^{1/n}}\left(R_a^T/R_a^M\right)}\right] \times\sqrt{2e^{-(p_m/C)^{1/n}}\left(\frac{R_a^T}{R_a^M}\right)+\left(\frac{R_a^T}{R_a^M}\right)^2} \tag{12}$$

Comparison of d and d_c reveals the following relationship:

$$\frac{d}{d_c} = \left[\frac{1+e^{2n}\left(R_a^T/R_a^M\right)}{1+e^{(p_m/C)^{1/n}}\left(R_a^T/R_a^M\right)}\right] \times\sqrt{\frac{2e^{-(p_m/C)^{1/n}}\left(R_a^T/R_a^M\right)+\left(R_a^T/R_a^M\right)^2}{2e^{-2n}\left(R_a^T/R_a^M\right)+\left(R_a^T/R_a^M\right)^2}} \tag{13}$$

Accordingly, the relationship d/d_c can be rewritten as follows by an elementary analysis of rigid plastic deformation in the

work-hardening material for a cantilever beam

$$\frac{d}{d_c}=\left[\frac{\sigma_i}{\sigma_u^0}\left(\frac{d_m}{d_x}\right)^2\right]^{1/n}\left[\frac{e^{2n}}{e^{(p_m/C)^{1/n}}}\right]^{2+1/n}\left(\frac{d_m}{d_x}\right) \tag{14}$$

The d_m/d_x can also be written as

$$\frac{d_m}{d_x}=\sqrt{\frac{e^{-(p_m/C)^{1/n}}+\left(R_a^T/R_a^M\right)}{e^{-2n}+\left(R_a^T/R_a^M\right)}} \tag{15}$$

Thus, σ_i/τ_s in the range of $R_a^T \le h \le (1-e^{-2n})R_a^M$ can be written as

$$\frac{\sigma_i}{\tau_s}=2e^{\left[(p_m/C)^{1/n}-2n\right](1+2n)}\left\{\left[1+e^{2n}\left(\frac{R_a^T}{R_a^M}\right)\right]\Big/\left[1+e^{(p_m/C)^{1/n}}\left(\frac{R_a^T}{R_a^M}\right)\right]\right\}^n\left\{\left[e^{-2n}+\left(\frac{R_a^T}{R_a^M}\right)\right]\Big/\left[e^{-(p_m/C)^{1/n}}+\left(\frac{R_a^T}{R_a^M}\right)\right]\right\}^{1+n/2}$$
$$\left\{\left[2e^{-(p_m/C)^{1/n}}\left(\frac{R_a^T}{R_a^M}\right)+\left(\frac{R_a^T}{R_a^M}\right)^2\right]\Big/\left[2e^{-2n}\left(\frac{R_a^T}{R_a^M}\right)+\left(\frac{R_a^T}{R_a^M}\right)^2\right]\right\}^{n/2} \tag{16}$$

and $h/R_a^M=1-e^{-(p_m/C)^{1/n}}$ where $p_m/C=\left(p_m/\sigma_u^0\right)$ $\left(\sigma_u^0/C\right)=\left(p_m/\sigma_u^0\right)(n/e)^n$ and $0\le\left(p_m/\sigma_u^0\right)\le(2e)^n$.

Condition 3: $h \ge (1-e^{-2n})R_a^M$

Under this condition, the surface layer of materials is fractured because $\left(p_m/\sigma_u^0\right)\approx(2e)^n$, i.e., $p_m\to\sigma_u=C(2n)^n$ or $\alpha\to1$. Therefore, the pure shear flow condition is induced in material subsurface, which always appears as a sticking state.

3 Results and discussions

3.1 Verification of the proposed model

The importance of modeling friction from the interface geometry between workpiece and tool has attracted the participation of many researchers. Osakada and Matsumoto [37] focused on the experimental observation of the effect of tool roughness on dry friction; and simultaneously made a case study to present the effect of tool roughness based on a serrated tool surface and similarity law in ring compression. However, this work did not establish the empirical relationship and not consider roughness of workpiece and material properties, such as strain hardening exponent. Lee et al. [38] proposed a friction model that considered lubricant viscosity and surface roughness for use in metal forming simulation. The relationship between friction coefficient and surface roughness of specimen was quantified by least squares method on the basis of experimental results,

$$\mu=0.24\lambda^2-0.346\lambda+0.252 \tag{17}$$

where λ is surface roughness of specimen. However, this work also did not consider material properties and tool roughness. Becker et al. [39] and Jeon and Bramley [41] described an alternative approach for describing friction in terms of geometric surface roughness of tools. A relationship between tool surface geometry and friction factor m was established by ring test,

$$m=-2.19\ln(0.0977\ln(t)-0.07\ln(a)+0.8086) \tag{18}$$

shown in [39] in which t is period and a is amplitude for a sinusoidal tool surface profile. This work emphasized the effect of tool roughness on dry friction, excluding the effect of material properties and roughness of workpiece. However, the present model, which accounts for adhesion and interference effects caused by surface roughness, was proposed to model sliding friction as measured by Amonton–Coulomb friction law. In this model, dry friction

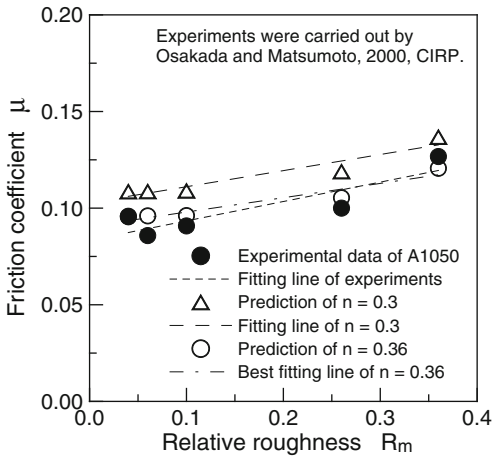

Fig. 3 Comparison between experiment and prediction of material A1050

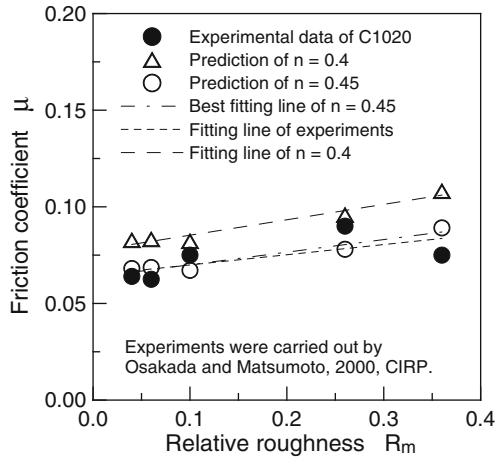

Fig. 4 Comparison between experiment and prediction of material C1020

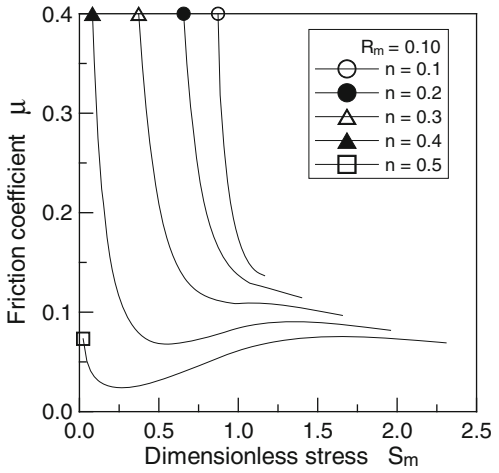

Fig. 6 Effects of dimensionless stress $S_m\left(=p_m/\sigma_u^0\right)$ on friction coefficient μ for various strain hardening exponent n under relative roughness R_m=0.1$\left(R_m=R_a^T/R_a^M\right)$

results from adhesion in normal contact and interference in lateral contact by contact interaction of roughness, which applied to actual physical properties of surface. A special feature is that a relative roughness R_a^T/R_a^M was defined to describe the contact roughness between workpiece and tools in contact layer. Moreover, in order to characterize contact friction accurately, the effect of material property, i.e., strain hardening exponent n, was also taken into account in this model. Clearly, the present model, shown in Eq. 5 and conditions 1–3, is a function of $\mu=f\left(p_m/\sigma_u^0, R_a^T/R_a^M, n\right)$, which compares more general and complete with the published models, such as Eq. 17 by Lee et al. [38] and Eq. 18 by Becker et al. [39] and Jeon and Bramley [41].

To investigate how roughness affects nominal friction, the published experiment by Osakada and Matsumoto [37] was first used to prove the proposed model. In this verification, the surface roughness of material R_a^M was assumed to be initial roughness $\overline{R}_a^M$.

Figure 3 shows the predicted results and experimental results for material A1050. The fitting lines (dashed lines) are quantified by least squares method on the basis of predicted and experimental results, in which the fitting line of experiment represents the result of Osakada and Matsumoto [37]. Clearly, friction coefficient μ correlates with relative roughness $R_m\left(=R_a^T/R_a^M\right)$. Although the n value is unclear in experiment, its common value approaches 0.3 in practical use. The n=0.3 prediction shows an overestimation. However, the n=0.36 prediction agrees well with the experiment. Accordingly, its trend approximates the experiment that obtained the best fit.

Figure 4 compares the prediction and experiment for material C1020. The fitting lines (dashed lines) are

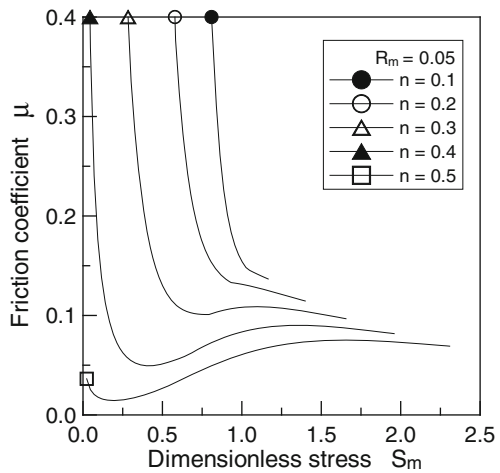

Fig. 5 Effects of dimensionless stress $S_m\left(=p_m/\sigma_u^0\right)$ on friction coefficient μ for various strain hardening exponent n under relative roughness R_m=0.05$\left(R_m=R_a^T/R_a^M\right)$

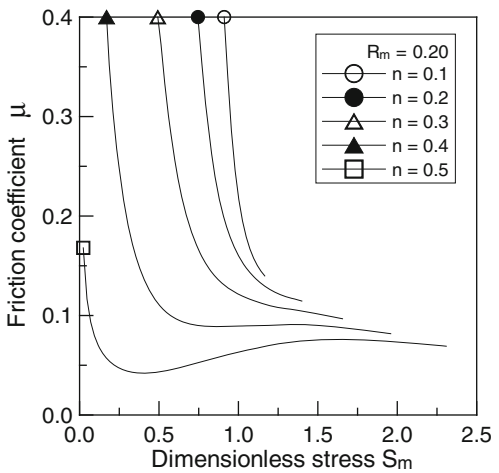

Fig. 7 Effects of dimensionless stress $S_m\left(=p_m/\sigma_u^0\right)$ on friction coefficient μ for various strain hardening exponent n under relative roughness R_m=0.2$\left(R_m=R_a^T/R_a^M\right)$

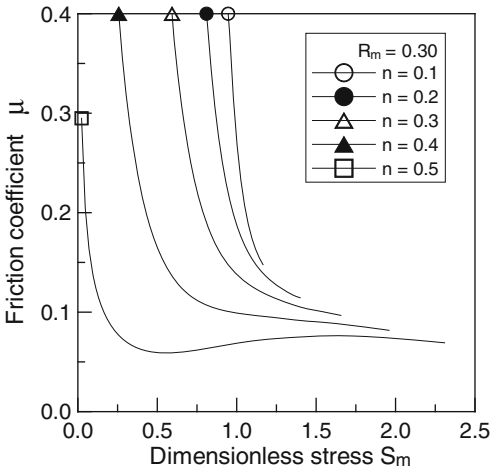

Fig. 8 Effects of dimensionless stress $S_m\left(=p_m/\sigma_u^0\right)$ on friction coefficient μ for various strain hardening exponent n under relative roughness R_m=0.3$\left(R_m=R_a^T/R_a^M\right)$

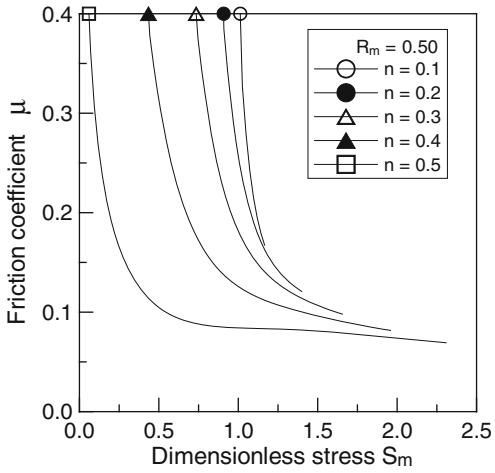

Fig. 10 Effects of dimensionless stress $S_m\left(=p_m/\sigma_u^0\right)$ on friction coefficient μ for various strain hardening exponent n under relative roughness R_m=0.5$\left(R_m=R_a^T/R_a^M\right)$

quantified by least squares method, in which the fitting line of experiment represents the result of Osakada and Matsumoto [37]. Friction coefficient μ clearly increases as relative roughness $R_m\left(=R_a^T/R_a^M\right)$ increases. The common n-value of C1020 approaches 0.4 in practical use and also obtains an overestimated prediction. However, the prediction of n=0.45 agrees well with the experiment. Accordingly, its trend approximates that in the experiment and has the best fit in this case.

Figures 3 and 4 show that the overestimations obtained in the simulations may have resulted from the assumption that $R_a^M \approx \overline{R}_a^M$ since R_a^M is very difficult to measure because of its highly variable deformation.

3.2 Effects of surface roughness and material property on dry friction

A second simulation was performed to determine how strain hardening exponent (material property) and roughness (surface condition) affect contact friction.

Figures 5, 6, 7, 8, 9, and 10 show the effects of dimensionless stress $S_m\left(=p_m/\sigma_u^0\right)$ on friction coefficient μ for varying strain hardening exponent n under a certain relative roughness $R_m\left(=R_a^T/R_a^M\right)$. Clearly, friction coefficient μ decreases as the dimensionless stress $S_m\left(=p_m/\sigma_u^0\right)$ increases at small n values. Under large n and small R_m values, friction coefficient μ first decreases. It then

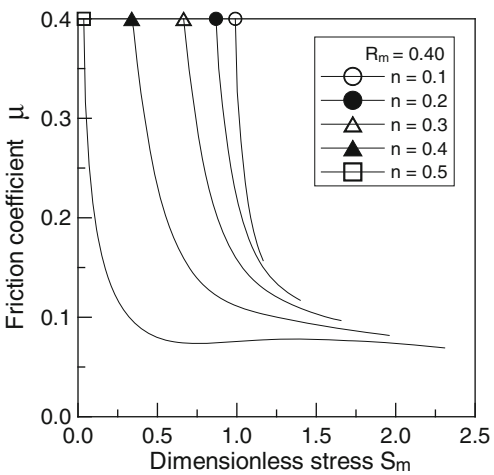

Fig. 9 Effects of dimensionless stress $S_m\left(=p_m/\sigma_u^0\right)$ on friction coefficient μ for various strain hardening exponent n under relative roughness R_m=0.4$\left(R_m=R_a^T/R_a^M\right)$

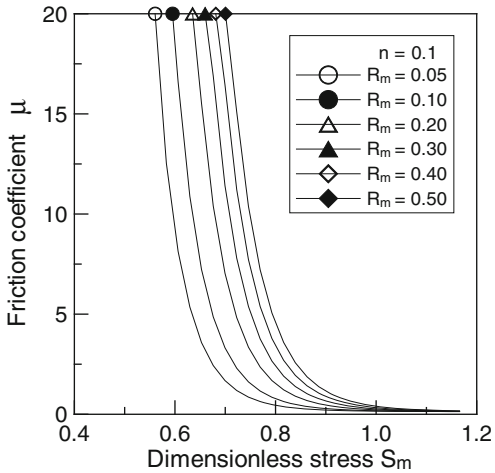

Fig. 11 Effects of dimensionless stress $S_m\left(=p_m/\sigma_u^0\right)$ on friction coefficient μ for various relative roughness $R_m\left(=R_a^T/R_a^M\right)$ under strain hardening exponent n=0.1

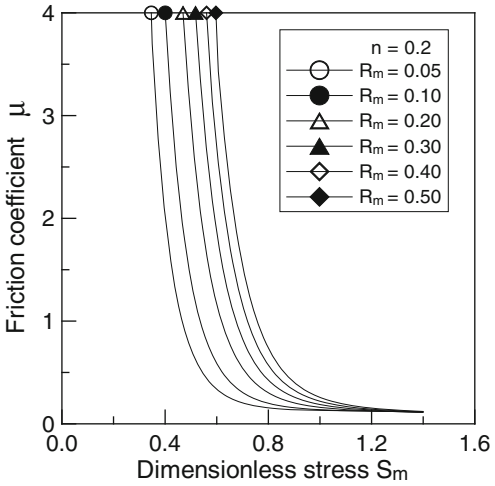

Fig. 12 Effects of dimensionless stress $S_m\left(=p_m/\sigma_u^0\right)$ on friction coefficient μ for various relative roughness $R_m\left(=R_a^T/R_a^M\right)$ under strain hardening exponent n=0.2

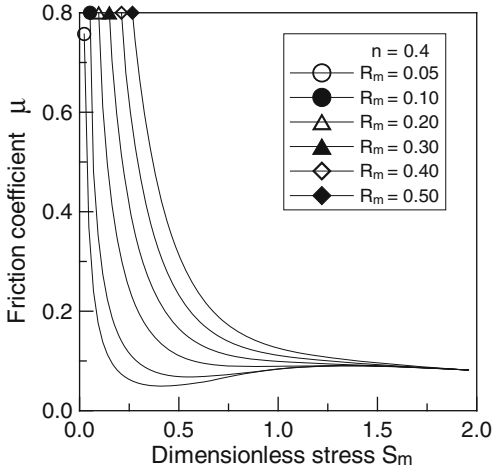

Fig. 14 Effects of dimensionless stress $S_m\left(=p_m/\sigma_u^0\right)$ on friction coefficient μ for various relative roughness $R_m\left(=R_a^T/R_a^M\right)$ under strain hardening exponent n=0.4

increases before it finally slightly decreases. However, this trend is less apparent as relative roughness $R_m\left(=R_a^T/R_a^M\right)$ increases since friction coefficient μ strictly decreases first and then slightly decreases with $S_m\left(=p_m/\sigma_u^0\right)$.

Figures 11, 12, 13, 14, and 15 show the effects of dimensionless stress $S_m\left(=p_m/\sigma_u^0\right)$ on friction coefficient μ for varying relative roughness $R_m\left(=R_a^T/R_a^M\right)$ under a certain strain hardening exponent n. Clearly, friction coefficient μ only decreases initially and then slightly decreases as the dimensionless stress $S_m\left(=p_m/\sigma_u^0\right)$ increases at small n values. Under large n and small R_m values, the friction coefficient μ first decreases and then increases before finally slightly decreases. However, this trend is less apparent as relative roughness $R_m\left(=R_a^T/R_a^M\right)$ increases such that friction coefficient μ simply decreases with $S_m\left(=p_m/\sigma_u^0\right)$.

4 Conclusions

1. The proposed model, which accounts for adhesion and interference effects resulting from surface roughness, was verified by the agreement between the predicted values and the experimental results.
2. Friction coefficient μ clearly increases as the relative roughness $R_m\left(=R_a^T/R_a^M\right)$, a measure of interference effect, increases. This study pursues this goal.
3. Notably, friction coefficient μ simply decreases as dimensionless stress $S_m\left(=p_m/\sigma_u^0\right)$ increases at small strain hardening exponent n values. Under the conditions of large n and small R_m values, friction coefficient μ first decreases before it increases. It then slightly decreases as dimensionless stress $S_m\left(=p_m/\sigma_u^0\right)$ increases.

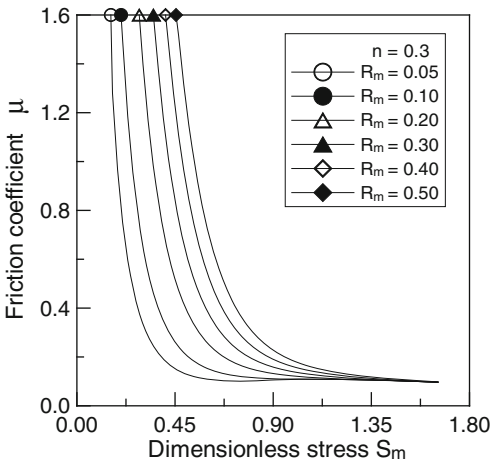

Fig. 13 Effects of dimensionless stress $S_m\left(=p_m/\sigma_u^0\right)$ on friction coefficient μ for various relative roughness $R_m\left(=R_a^T/R_a^M\right)$ under strain hardening exponent n=0.3

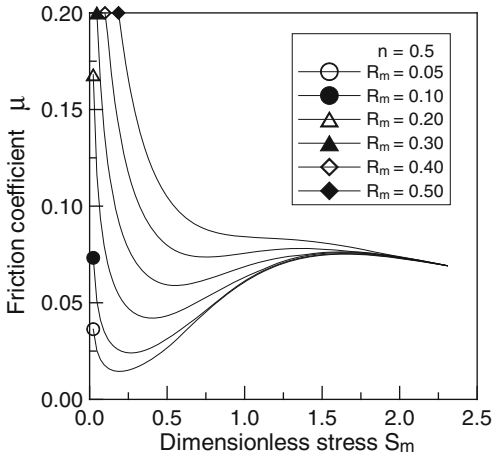

Fig. 15 Effects of dimensionless stress $S_m\left(=p_m/\sigma_u^0\right)$ on friction coefficient μ for various relative roughness $R_m\left(=R_a^T/R_a^M\right)$ under strain hardening exponent n=0.5

However, this trend diminishes as relative roughness $R_m \ (= R_a^T / R_a^M)$ increases since friction coefficient μ simply decreases.

Acknowledgments The author would like to thank the National Science Council of the Republic of China for financially supporting this research under Contract No. NSC 98-2221-E-149-003. The author is grateful to Dr. C-W Yen for helpful discussions. Ted Knoy is appreciated for his editorial assistance.

References

1. Leu DK (2011) Evaluation of friction coefficient using indentation model of Brinell hardness test for sheet metal forming. J Mech Sci Tech (in press)
2. Leu DK (2010) Evaluation of friction coefficient using simplified deformation model of plastic hemispherical contact with a rigid flat. J Mech Sci Technol 24(8):1697–1707
3. Greenwood JA, Williamson JBP (1966) Contact of nominally flat surfaces. Proc R Soc London Ser A 295:300–319
4. Abbott EJ, Firestone FA (1933) Specifying surface quality—a method based on accurate measurement and comparison. Mech Eng Am Soc Mech Eng 55:569–572
5. Chang WR, Etsion I, Bogy DB (1988) Static friction coefficient model metallic rough surfaces. ASME J Tribol 110:57–63
6. Kogut L, Etsion I (2003) A semi-analytical solution for the sliding inception of a spherical contact. ASME. J Tribol 125:499–506
7. Kogut L, Etsion I (2004) A static friction model for elastic-plastic contacting rough surfaces. ASME J Tribol 126:34–40
8. Cohen D, Kligerman Y, Etsion I (2009) The effect of surface roughness on static friction and junction growth of an elastic-plastic spherical contact. ASME. J Tribol 131:021404
9. Bowden FP, Tabor D (1953) The friction and lubrication of solids. Clarendon, Oxford, pp 98–100
10. Orowan E (1941) The calculation of roll pressure in hot and cold flat rolling. Proc Inst Mech Eng 150:140–167
11. Wanheim T, Bay N, Petersen AS (1974) A theoretically determined model for friction in metal working processes. Wear 28:251–258
12. Bay N, Wanheim T (1976) Real area of contact friction stress at high pressure sliding contact. Wear 38:201–209
13. Wanheim T, Bay N (1978) A model for friction in metal forming processes. CIRP Annal 27:189–194
14. Bay N (1987) Friction stress and normal stress in bulk metal forming process. J Mech Work Tech 14:203–223
15. Greenwood JA, Rowe GW (1965) Deformation of surface asperities during bulk plastic flow. J Appl Phys 36:667–668
16. Sheu S, Wilson WRD (1983) Flattening of workpiece surface asperities in metal forming. Proc NAMRC XI (SME):172–178
17. Wilson WRD, Sheu S (1988) Real area of contact and boundary friction in metal forming. Int J Mech Sci 30(7):475–489
18. Sutcliffe MFP (1988) Surface asperity deformation in metal forming processes. Int J Mech Sci 30(11):847–868
19. Azushima A (1995) Direct observation of contact behaviour to interpret the pressure dependence of the coefficient of friction in sheet metal forming. Annals of the ClRP 44(1):209–212
20. Gong H, Lou Z, Zhang Z (2004) Studies on the friction and lubrication characteristics in the sheet steel drawing process. J Mater Process Technol 151:328–333
21. Xie Y, Wilfams JA (1996) The prediction of friction and wear when a soft surface slides against a harder rough surface. Wear 196:21–34
22. Lovell MR, Deng Z (1999) Experimental investigation of sliding friction between hard and deformable surfaces with application to manufacturing processes. Wear 236:117–127
23. Cho H, Ngaile G (2003) Simultaneous determination of flow stress and interface friction by finite element based inverse analysis technique. Annals of the CIRP 52(1):221–224
24. Carpinteri A, Paggi M (2005) Size-scale effects on the friction coefficient. Int J Solids Struct 42:2901–2910
25. Stachowiak GW, Batchelor AW (2005) Engineering tribology, 3rd edn. Elsevier, Butterworth
26. Lanzon JM, Cardew-Hall MJ, Hodgson PD (1998) Characterising frictional behaviour in sheet metal forming. J Mater Process Technol 80–81:251–256
27. Weidel S, Enget U (2007) Surface characterization in forming processes by functional 3D parameters. Int J Adv Manuf Technol 33(1–2):130–136
28. Menezes PL, Kishore KSV, Lovell MR (2010) Response of materials as a function of grinding angle on friction and transfer layer formation. Int J Adv Manuf Technol 49(5–8):485–495
29. Menezes PL, Kumar K, Kishore, Kailas SV (2009) Influence of friction during forming processes—a study using a numerical simulation technique. Int J Adv Manuf Technol 40(11–12):1067–1076
30. Menezes PL, Kishore, Kailas SV (2009) Influence of roughness parameters and surface texture on friction during sliding of pure lead over 080M40 steel. Int J Adv Manuf Technol 43(7–8):731–743
31. Rigney DA (2000) Transfer, mixing and associated chemical and mechanical processes during sliding of ductile materials. Wear 245:1–9
32. Bonny K, De Baets P, Vleugels J, Salehi A, Van der Biest O, Lauwers B, Liu W (2008) EDM machinability and frictional behavior of ZrO_2-WC composites. Int J Adv Manuf Technol 41 (11–12):1085–1093
33. Diaz de Cerio MJ, Fuentes GG, Martinez R, Rodriguez RJ, Spain E, Housden J, Qin Y, Hörnig W (2010) Temperature-dependent contact phenomena of PVD- and CVD-deposited DLC films sliding on the thin aluminium foil. Int J Adv Manuf Technol 47(9–12):931–936
34. Edwards CM, Halling J (1968) An analysis of the plastic interaction of surface asperities and its relevance to the value of the coefficient of friction. J Mech Eng Sci 10:101–110
35. Wanheim T, Abildgaard T (1980) A mechanism for metallic friction. Proc 4th Int Conf Prod Eng Tokyo: 122–127
36. Avitzur B, Van Tyne CJ, Luo ZJ, Tang CR (1984) A model for the simulation of friction between dies and workpieces. Proc 1st Int Con on Adv Technology and Plasticity. Tokyo: 200–207
37. Osakada K, Matsumoto R (2000) Fundamental study of dry metal forming with coated tool. CIRP Annals 49:161–164
38. Lee BH, Keum YT, Wagoner RH (2002) Modeling of the friction caused by lubrication and surface roughness in sheet metal forming. J Mater Process Technol 120–131:60–63
39. Becker P, Jeon HJ, Chang CC, Bramley AN (2003) A geometric approach to modeling friction in metal forming. CIRP Annals 52:209–212
40. Mahrenholtz O, Bontcheva N, Lankov R (2005) Influence of surface roughness on friction during metal forming processes. J Mater Process Technol 159(1):9–16
41. Jeon J, Bramley AN (2007) A friction model for microforming. Int J Adv Manuf Technol 33:125–129
42. Menezes PL, Kishore KSV (2008) Influence of roughness parameters on coefficient of friction under lubricated condition. Sādhanā 33(3):181–190
43. Shaw MC (1970) Metal cutting principles. Oxford Press, Oxford
44. Dieter GE (1976) Mechanical metallurgy (second edition). New York, McGraw Hill, pp 389–394
45. Leu DK (2009) A simple dry friction model for metal forming process. J Mater Process Technol 209:2361–2368